Intermolecular Effects on Tunneling through Acenes in Large-Area and Single-Molecule Junctions

Liu, Yuru; Ornago, Luca ; Carlotti, Marco; Al, Yong; abbasi, maria el; Soni, Saurabh; Asyuda, Andika; Zharnikov, Michael; Zant, Herre S. J. van der; Chiechi, Ryan

Published in:
The Journal of Physical Chemistry. C: Nanomaterials and Interfaces

DOI:
10.1021/acs.jpcc.0c05781

Publication date:
2020

THE JOURNAL OF PHYSICAL CHEMISTRY C

pubs.acs.org/JPCC

Article

Intermolecular Effects on Tunneling through Acenes in Large-Area and Single-Molecule Junctions

Yuru Liu, Luca Ornago, Marco Carlotti, Yong Ai, Maria El Abbassi, Saurabh Soni, Andika Asyuda, Michael Zharnikov, Herre S. J. van der Zant,* and Ryan C. Chiechi*

Cite This: J. Phys. Chem. C 2020, 124, 22776−22783

Read Online

ACCESS | Metrics & More | Article Recommendations | Supporting Information

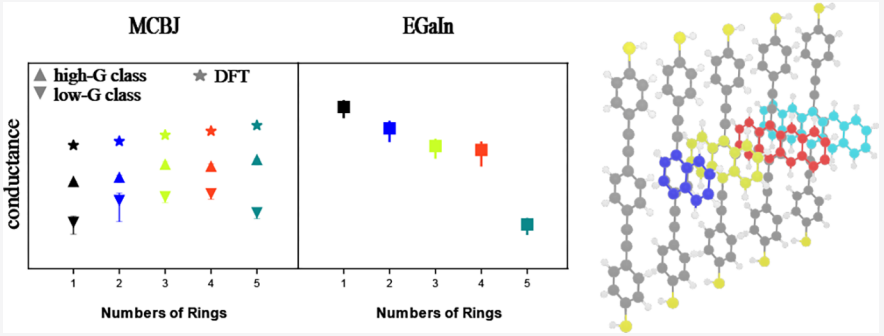

ABSTRACT: This paper describes the conductance of single-molecules and self-assembled monolayers comprising an oligophenyleneethynylene core, functionalized with acenes of increasing length that extend conjugation perpendicular to the path of tunneling electrons. In the Mechanically Controlled Break Junction (MCBJ) experiment, multiple conductance plateaus were identified. The high conductance plateau, which we attribute to the single molecule conformation, shows an increase of conductance as a function of acene length, in good agreement with theoretical predictions. The lower plateau is attributed to multiple molecules bridging the junctions with intermolecular interactions playing a role. In junctions comprising a self-assembled monolayer with eutectic Ga−In top-contacts (EGaIn), the pentacene derivative exhibits unusually low conductance, which we ascribe to the inability of these molecules to pack in a monolayer without introducing significant intermolecular contacts. This hypothesis is supported by the MCBJ data and theoretical calculations showing suppressed conductance through the **PC** films. These results highlight the role of intermolecular effects and junction geometries in the observed fluctuations of conductance values between single-molecule and ensemble junctions, and the importance of studying molecules in both platforms.

INTRODUCTION

Understanding the correlation between the chemical structure of molecules and charge transport through molecular junctions is one of the biggest challenges of molecular electronics.[1] By chemical design, several devices with functionality, such as rectification and switching, have already been demonstrated.[2−4] The synthetic control over the structure of organic molecules makes them useful functional elements,[5] particularly, π-conjugated molecules, because their electronic delocalization facilitates charge transport in both hopping and tunneling processes. Quantum interference (QI) effects can also be accessed readily by synthetically tuning the wave functions of the π system.[6] These effects have been predicted theoretically and observed experimentally in π-conjugated molecules that exhibit cross-conjugation,[7−12] meta-substitution,[13,14] and noncovalent spatial overlap.[6,15,16]

Oligo(phenyleneethynylene) (OPE) compounds and their derivatives are a widely used class of functional π-conjugated molecular wires, rigid, and rod-like molecules, making them the building blocks of large-area and single-molecule junctions.[16−19] Oligoacenes are another class of rigid, planar, aromatic, and linear π-conjugated molecular wires. One interesting feature of oligoacene is its exponentially narrow HOMO−LUMO band gap,[20] which attracts lots of researches on their electronic properties.[21−23]

Here, we study five OPE derivatives in which the central benzene ring is replaced by a series of oligoacenes: naphthalene (**NP**), anthracene (**9,10-AC**), tetracene (**TC**), and pentacene (**PC**). As shown in Figure 1, this functionalization strategy extends π-conjugation perpendicular to the long axis of the molecular wire, like in cruciforms.[24,25] This acene series

Received: June 25, 2020
Revised: September 14, 2020
Published: September 14, 2020

https://dx.doi.org/10.1021/acs.jpcc.0c05781
J. Phys. Chem. C 2020, 124, 22776−22783

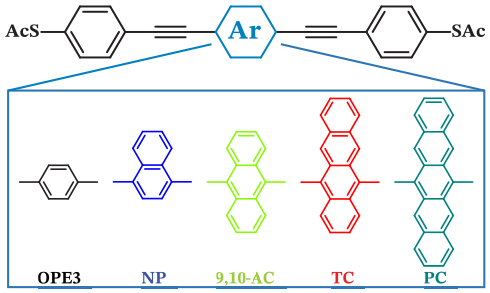

Figure 1. Chemical structures of **OPE3**-like acene series.

maintains the same linear conjugation pattern and length between the thiol anchors, allowing the interrogation of the effects of extended conjugation in both large-area and single-molecule junctions without changing the width of the tunneling barrier or introducing heteroatoms.

METHODS AND MATERIALS

Chemicals and Synthesis. The synthesis of **OPE3**, **NP** and **9,10-AC** is described elsewhere.[26] All compounds were stored in nitrogen-flushed vials and in the dark. The synthesis of **TC** and **PC** were performed according to procedures highlighted in Figure S1 and Figure S2 respectively. All the synthesis procedures are described in the Supporting Information.

Self-Assembled Monolayers. To ensure that high-quality self-assembled monolayers (SAMs) are formed, we used an *in situ* deprotection strategy that is optimized for large, π-conjugated molecules[16,17] to grow SAMs directly on ultra-smooth Au substrates prepared by template-stripping (Au^{TS}).[27] A 100 nm layer of Au (99.99%) was deposited by thermal deposition at 10^{-7} mbar onto a 3 in. silicon wafer (without adhesion layer). Glass substrates (1 cm × 1 cm) were glued onto deposited metal by using UV-curable optical adhesive (Norland 61) with 300 s exposure of UV. All SAMs were formed by incubating the thioacetate precursors with 1 cm × 1 cm template-stripped Au surfaces (100 nm thick) overnight in 3 mL of 50 μM solution of the respective compound in freshly distilled toluene followed by addition of 0.05 mL of 17 mmol dm^{-3} diazabicylcoundec-7-ene solution in toluene 1 h prior the measurement. The substrates were then rinsed with ethanol and let to dry for 10 min.

Surface Characterization. Angle-resolved XPS (ARXPS) measurement were performed using a VG Microtech spectrometer with a hemispherical electron analyzer (Clam 100), and a Mg Kα (1253.6 eV) X-ray source. The measurement procedure and data analysis were following the method stated in the experimental section in a previous paper.[28] Synchrotron-based X-ray photoelectron spectroscopy (XPS) measurements were performed at the HE-SGM beamline (bending magnet) of the German synchrotron radiation facility BESSY II in Berlin using a custom-designed experimental station.[29] The spectra were collected with a SCIENTA SES200 electron energy analyzer, in normal emission geometry. The synchrotron light served as the primary X-ray source. The photon energy was set either to 350 or 580 eV depending on the acquisition range. The energy resolution was 0.3 and 0.6 eV, respectively. The binding energy scale of the spectra was referenced to the Au $4f_{7/2}$ peak at 84.0 eV.[30]

EGaIn Measurement. To minimize the oxidative damage to the compounds and SAMs, sample preparation, handing, and measurement with the EGaIn setup were all performed in a nitrogen flow box with a controlled O_2 level between 1 and 3% (some O_2 is necessary to form tips of EGaIn) and humidity below 10%. At least 20 junctions were measured on each of at least three substrates per molecule (12 scans from 0 V → 1 V → − 1 V → 0 V, steps of 0.05 V) for a total of at least 600 traces per SAM. A new EGaIn tip was prepared every 5−8 junctions and flattened by gently pushing it on a Si wafer a few times according to the procedure reported by Simone et al.[31] The details of the EGaIn setup are described elsewhere.[9]

MCBJ Measurement. In the MCBJ experiment, a lithographically fabricated nanoscale gold wire was patterned on a flexible substrate. Electrodes were first characterized without molecules to ensure that they were clean (in which case a clear peak at 1 G_0 is observed, indicative of atomically sharp electrodes, followed by exponential decay of conductance with increasing displacement). Then, a droplet of the solution that contained the molecules was deposited on the electrodes (0.1 mM in dichloromethane, with 0.5 mM of tetrabutylammonium hydroxide to favor removal of the acetate protection). After solvent evaporation, thousands of traces are recorded consecutively. The measurements were performed in air at room temperature, using a bias voltage of 100 mV and 200 V/s piezo actuation speed. The measurements were repeated on a total of two devices (with four junctions each), measuring at least 7000 consecutive traces on a single junction for each sample. A detailed description of this technique and the experimental setup has been given previously.[32]

Theoretical Methods. DFT calculations were performed using the ORCA 4.10 software package.[33,34] The molecules terminated with thiols were first optimized by BP/def2-SVP in the gas phase; then the molecules were attached to two pyramidal Au clusters via the terminal sulfur atoms. Single-point energy calculations were performed on this model junction using B3LYP/G and LANL2DZ basis sets according to literature procedures to compute the energy levels.[35] Transmission curves were computed in ARTAIOS using outputs from B3LYP/G(LANL2DZ) calculations based on the minimized geometries.[36] Slip-stack transmission calculations were performed using the *BAND* module of Amsterdam Density Functional (ADF) quantum chemistry program.[37]

RESULTS AND DISCUSSION

Transmission Spectra. Figure 2 shows the transmission spectra for the acene series in single-molecule, Au/molecule/Au geometry. The spectra show that the frontier orbital gap (E_g) between the highest occupied π-state (HOPS) and the lowest unoccupied π-state (LUPS) decreases as the conjugation length increases from **OPE3** to **PC**. Large, positive resonances move toward the Fermi level E_F with increasing conjugation length, reflecting the shrinking of frontier molecular orbital gap; however, on the basis of these simulated transmission spectra, the low-bias conductance, which is determined by transmission at E_F, is not expected to change much as the transmission probability near E_F increases by only a factor of 5 when going from **OPE3** to **PC**. Thus, the NEGF-DFT simulation predicts the experimental trend in low-bias conductance to increase moderately and continuously from **OPE3** to **PC** as E_g decreases.

EGaIn Junctions. We measured tunneling charge-transport through large-area junctions comprising **OPE3**, **NP**, **9,10-AC**,

https://dx.doi.org/10.1021/acs.jpcc.0c05781
J. Phys. Chem. C 2020, 124, 22776−22783

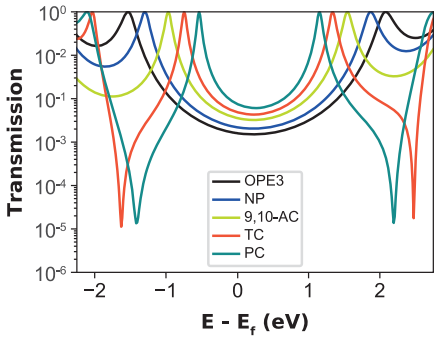

Figure 2. Transmission spectra calculated for **OPE3**, **NP**, **9,10-AC**, **TC**, and **PC**. The *x*-axis is referenced to an approximate Fermi level of −4.3 eV for EGaIn (see ref 38).

TC, and **PC** molecular wires using conformal eutectic Ga−In (EGaIn) contacts as top electrodes.[39] Figure 3 shows the

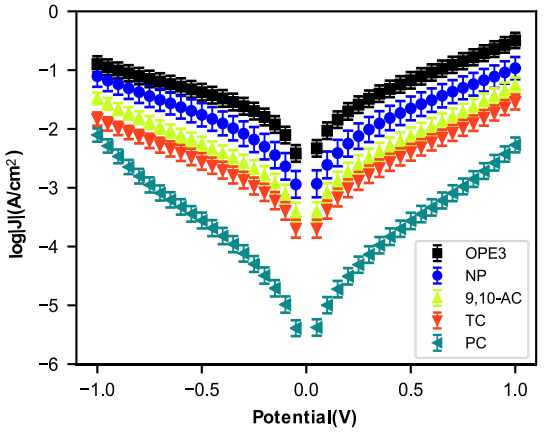

Figure 3. Plots of log |**J**| (the units of *J* are A cm^{-2}) versus *V* for SAMs using EGaIn top-contacts (Au^{TS}/SAM//EGaIn): black squares for **OPE3**, blue circles for **NP**, lemon-yellow up-triangle for **9,10-AC**, red down-triangle for **TC**, and dark green left-triangle for **PC**. Each data point is the mean from a Gaussian fit to a histogram of log |**J**|.

current-density versus voltage (J/V) curves for the acene series. Current density shows a slightly descreasing trend: **OPE3** > **NP**, **9,10-AC** to **TC**. However, the low-bias conductance value of **PC** is significantly lower than the rest of the series, despite having the smallest E_g. While this observation could result from poor quality SAMs, spectroscopic evidence suggests that SAMs of **PC** do not differ significantly from the rest (see below). These results deviate from those predicted by the transmission spectra in Figure 2, suggesting that the NEGF-DFT simulations are not capturing a key physical detail that is intrinsic either to the molecules or the SAMs.

SAM Characterization. We characterized SAMs of the acene series molecules by several complementary techniques, including atomic force microscopy (AFM) and synchrotron-based X-ray photoelectron spectroscopy (XPS). AFM images (Figure S10) show that the surface morphologies of the SAMs are similar. The effective thicknesses of the acene SAMs were measured by angle-resolved XPS in a home-built machine (see Supporting Information subsection 2.2).[40] The results are summarized in Table S5 along with the value for aliphatic octadecanethiol SAM, **SC18** as a reference.[41] The thickness values for all acene SAMs, except for **9,10-AC**, are comparable, but slightly higher than that for **SC18** in spite of the similar molecular lengths. On the one hand, this difference may be related to the different attenuation lengths of the photoelectrons for aliphatic and aromatic compounds. On the other hand, it can result from the sensitivity of acenes to oxidation during the unavoidable, brief exposure to air upon loading the samples into the vacuum chamber of the XPS spectrometer.[42,43] The somewhat higher thickness of **9,10-AC** can be tentatively explained by deprotection agent contamination for this particular sample. Most important, however, is that the thickness of **PC** was very similar to those of the other SAMs.

Further, the acene SAMs, except for **OPE3** studied in detail before,[16] were characterized by synchrotron-based XPS. Representative C 1s XP spectra of these SAMs, measured with an energy resolution of approximately 0.3 eV and presented in Figure 4, show a single, nearly symmetric peak

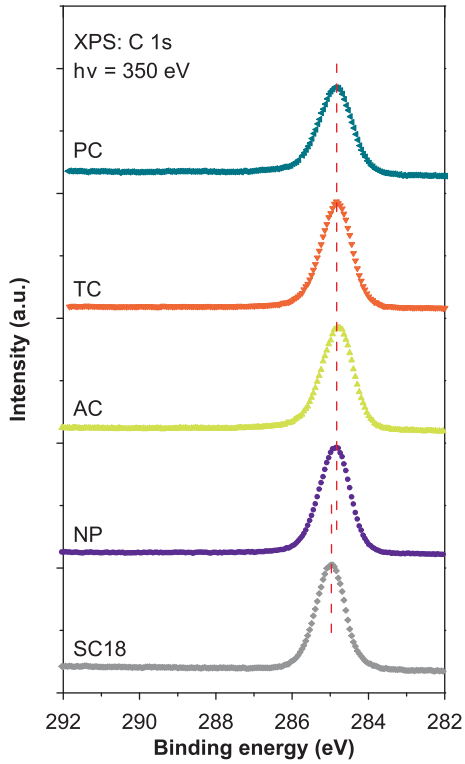

Figure 4. C 1s XP spectra of **NP**, **9,10-AC**, **TC**, and **PC** and reference **SC18** SAMs on Au/mica substrates. The positions of the observed peak are marked by red dash lines.

associated with the backbone of the acene molecules. As expected for such molecules,[44] this peak is shifted to lower binding energy (284.8 eV) as compared to that for **SC18** (285.0 eV). Most important, however, is the absence of any perceptible signals associated with the presence of oxygen-containing and nitrogen-containing contaminants. In addition to this qualitative analysis, the packing density of the acene SAMs was roughly estimated. The results are presented in Table S5. The values vary to some extent over the series but are similar to each other, including **PC**. Thus, the morphology of the SAMs alone cannot explain the abnormally low conductance of **PC**.

MCBJ Measurement. Having established that the unexpected experimental trends in conductance are most likely not due to artifacts in the SAMs, we turned to single-molecule measurements to disentangle the properties of

https://dx.doi.org/10.1021/acs.jpcc.0c05781
J. Phys. Chem. C 2020, 124, 22776−22783

individual molecules from intermolecular effects present in SAMs. Thus, in parallel with SAM measurements, single molecular scale investigation of the acene-substituted **OPE3**s was performed using the mechanically controllable break-junction technique (MCBJ).[32,45] **OPE3** and their derivatives have been extensively studied in single-molecule junctions, and they show a conductance plateau at around 1×10^{-4} G_0.[46] However, additional lower conductance features have been reported, which at least in part are thought to be caused by the formation of $\pi-\pi$ stacked dimers in which each molecule is coupled to one electrode.[18,47] In the measurements performed on the series of acene substituted **OPE3**s, a high-conductance plateau could be identified in all cases, together with low-conductance features (Figure 5a, Supporting Information subsection 1.4 for all measurements). The most-probable conductance values obtained by fitting the data are reported in Table 1.

A reference-free clustering algorithm was used to better identify the molecular features emerging from the measurements, similar to previous reports.[48,49] In this way, three main categories of classes were identified: the high-conductance plateau, the low-conductance features, and traces with no clear signature of a molecule ("empty" traces). An example of the resulting histograms of the high-conductance class is given in Figure 5b. All measurements consistently showed this class, whose conductance at the peak in the 1D histograms follows the trend **OPE3** < **NP** < **9,10-AC** ≈ **TC** < **PC** (Figure 5c, Table 1), in agreement with the transmission calculated for this series of molecules (Figure 2). Note that the conductance peak in the 1D histograms is more prominent and narrower in the high-conductance class than in the unfiltered data, yielding a more accurate estimation of the most-probable molecule conductance. On the other hand, the low-conductance features do not appear to follow a clear trend (Table 1): sometimes they appear as slanted traces at $\approx 10^{-6}$ G_0 (as for **OPE3**), as shorter plateaus at around 10^{-5} G_0 (as for **TC**), as long (>2 nm) straight plateaus in the 10^{-5}–10^{-6} G_0 range (mostly for **PC**), or even as combinations of the aforementioned behaviors (**NP** and **9,10-AC**) (see Supporting Information subsection 1.4, Table S4).

Intermolecular Interactions. Figure 6 compares the trends in low-bias conductance for the acene series in single-molecule MCBJs and SAMs in EGaIn junctions (extracted from the low-bias region; see Supporting Information subsection 1.3). While the MCBJ data show both high- and low-conductance peaks for each acene, the EGaIn data show one value per molecule. The EGaIn values are clustered together, with the exception of **PC**; the conductance of this molecule is significantly less with respect to the others. We further plot the conductance of individual molecules at low bias based on J/V results obtained from EGaIn measurements and packing density results from XPS (see Supporting Information subsection 3.1). Figure S11 shows the same conductance trend as shown in Figure 6b. The trend in the high-conductance values in the MCBJs data are in agreement with the transmission calculations presented in Figure 2. In contrast, the low conductance plateau and the EGaIn data are not compatible with these calculations, suggesting that the experiments are capturing effects in addition to transport through isolated single-molecules.

It is known that, in MCBJs, intermolecular interactions can suppress the conductance significantly when two molecules contact each other in a single junction[50] and are not anchored

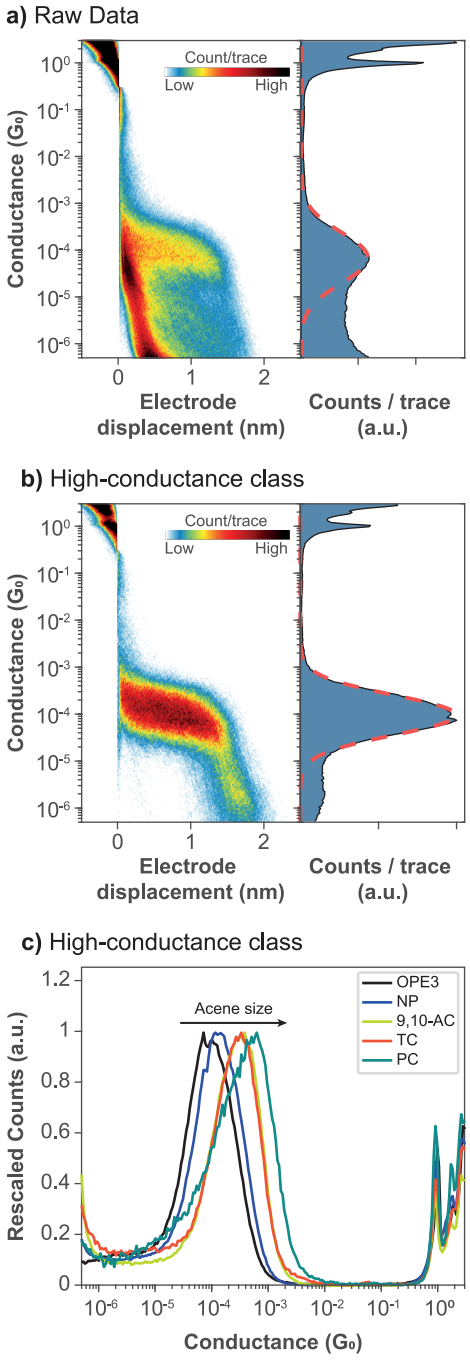

Figure 5. (a) 2D conductance–displacement (left panel) and 1D conductance (right panel) histograms of **OPE3**. (b) 2D conductance–displacement (left panel) and 1D conductance (right panel) histograms of the corresponding high-conductance class extracted through clustering. (c) 1D conductance histograms of the high-conductance class for all molecules of the studied series. Each histogram includes all measurements from the corresponding molecule obtained after clustering. Counts were rescaled by peak height.

to the two sides of the electrodes. Ordinarily, in SAMs, molecules are sufficiently noninteracting that they behave as independent tunnel junctions placed in parallel. However, the conjugation in the acene series increases parallel to the surface (perpendicular to the S–S axis) such that lateral interactions become more likely. As is shown schematically in Figure S12, it is hard to arrange **TC** and **PC** on an Au(111) surface without

https://dx.doi.org/10.1021/acs.jpcc.0c05781
J. Phys. Chem. C 2020, 124, 22776–22783

Table 1. Average Most-Probable Conductance (Plus−Minus Standard Deviation) for Each Molecule

	raw data	high-conductance class	low-conductance class
OPE3	$(7.6 \pm 1.90) \times 10^{-5}$	$(9.4 \pm 0.10) \times 10^{-5}$	$(3.8 \pm 2.30) \times 10^{-6}$
NP	$(1.1 \pm 0.30) \times 10^{-4}$	$(1.3 \pm 0.20) \times 10^{-4}$	$(2.1 \pm 1.70) \times 10^{-5}$
9,10-AC	$(3.1 \pm 1.0) \times 10^{-4}$	$(3.6 \pm 0.80) \times 10^{-4}$	$(2.8 \pm 1.0) \times 10^{-5}$
TC	$(2.1 \pm 0.60) \times 10^{-4}$	$(3.1 \pm 0.60) \times 10^{-4}$	$(3.6 \pm 1.30) \times 10^{-5}$
PC	$(3.6 \pm 0.70) \times 10^{-4}$	$(5.2 \pm 0.30) \times 10^{-4}$	$(8.0 \pm 3.0) \times 10^{-6}$

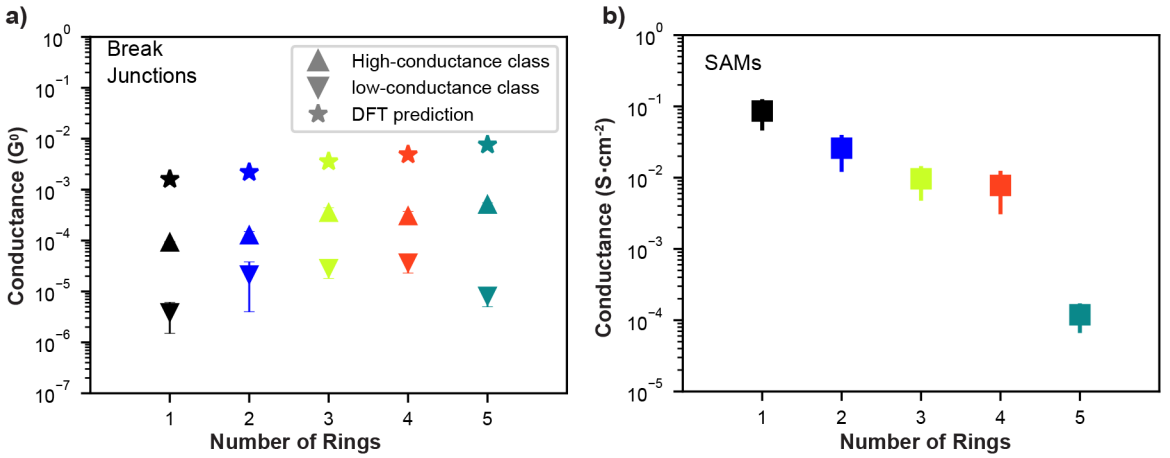

Figure 6. (a) Experimental MCBJ (triangles) and simulated (stars) conductances of single-molecule junctions: up-triangles are from the high-conductance plateaux, down-triangles are from the low-conductance plateaux, and stars are conductances as $G = G_0T(0)$ from the DFT simulations shown in Figure 2. (b) Conductances of SAMs of the acence series, extracted from the J/V traces of EGaIn data in Figure 3.

significant intermolecular contacts at the acene functionalities. **TC** still has some freedom to avoid intermolecular interaction, and junctions with this molecule may be a mixture of tunneling pathways from noninteracting and interacting molecules. It should be noted that a small fraction of molecules in a high-conductance state can increase the overall conductance of a junction, masking the presence of low-conductance molecular states,[51−53] as is described in more detail in Supporting Information subsection 3.3 and Figure S13. The small decrease in conductance present in Figure S12 for **TC** and to a lesser extent for **PC** may reflect this competition between the two states. Thus, we hypothesize that, as the acene moiety becomes longer, intermolecular interactions become increasingly more important and that the **PC** molecules interact strongly enough that they no longer act as tunneling junctions in parallel but exhibit the same suppression of conductance that manifests as multiple conductance plateaus in MCBJs.

For more insights into the molecular interactions, we computed the normalized differential conductance (NDC) for the acene series of EGaIn junctions, shown as heatmaps in Figure 7. For **OPE3**, **NP**, **9,10-AC**, and **TC** a U-shaped curve is observed indicative of nonresonant tunneling. For **PC** a distinctively different shape is found, especially around zero-bias where the curve is more V shaped. The qualitative difference between **PC** and the rest of the series confirms that the suppression of conductance correlates to a difference in bias dependence, which would not be the case for multilayers or other artifacts that simply increase the tunneling distance. V-shaped curves, on the other hand, have been observed before and ascribed to destructive quantum-interference (QI) effects in SAMs.[11,12,16,54]

This V-shaped feature is not present in the transmission curves of Figure 2 because those calculations are based on a single-molecule junction in vacuum. Because they are periodic,[55,56] simulations on SAM-based junctions require highly crystalline, particularly well-ordered SAMs—criteria that are not met by the acene series. However, atomistic simulations were performed on a metal−molecular metal model junction comprising two molecules trapped between metallic leads and semi-infinite, periodic electrodes using ADF-BAND, implementing the nonequilibrium Green's function approach with DFT[37] (Figure S17 and Figure S18). Here, we put a slip-stack geometry of two **PC** molecules between metal electrodes. Figure S19 shows suppressed transmission near E_F and a broadening of antiresonances in the slip-stack geometry compared to single molecules, suggesting that a SAM comprising **PC** molecules in contact with each other would exhibit lower conductance than a SAM comprising non-interacting **PC** molecules. Figure S20 shows a theoretical prediction of QI by looking at the orbital coefficients of the molecules,[57,58] where we see QI features in the pentacene dimer geometry but not in individual pentacene molecules. Together with the trends in conductance and the NDC plots, we ascribe the suppressed conductance in junctions comprising SAMs of **PC** to a specific packing geometry involving intermolecular $\pi-\pi$ interactions.

CONCLUSION

In both the MCBJs and EGaIn measurements we find that increasing the π surface area of molecules promotes intermolecular interactions that suppress the conductance compared to the case of a single-molecule bridging the electrodes. In MCBJs, this single-molecule configuration and the configurations involving two or more molecules lead to distinct features in the conductance histograms. In EGaIn junctions, where molecules seek a thermodynamic-minimum packing, **PC** in the series shows a suppression of conductance that cannot be explained by bond topology or the formation of

https://dx.doi.org/10.1021/acs.jpcc.0c05781
J. Phys. Chem. C 2020, 124, 22776−22783

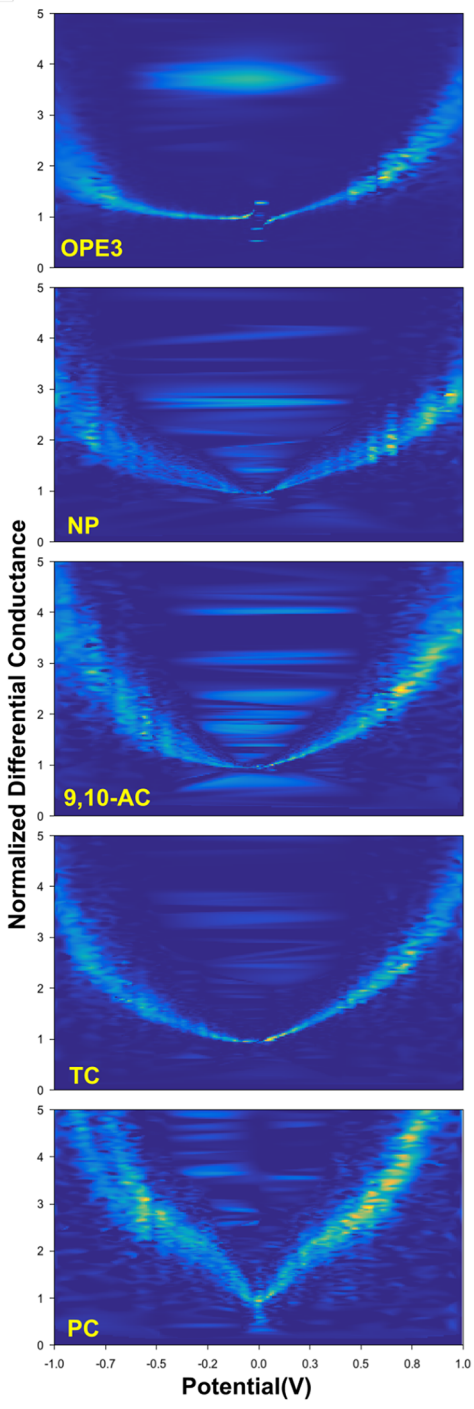

Figure 7. Normalized differential conductance heatmap plots of Au^{TS}/SAMs//EGaIn junctions comprising (a) **OPE3**, (b) **NP**, (c) **9,10-AC**, (d) **TC**, and (e) **PC**. The *Y*-axis is normalized differential conductance $\log|dJ/dV|$, and the *X*-axis is potential. The colors correspond to the frequencies of the histogram and the lighter color represents higher frequencies.

multilayers, suggesting the presence of molecular interactions, which is especially strong for the extended pentacene cores. Differential conductance plots of this molecule are consistent with the presence of a destructive QI feature in the bias window, which is supported by DFT calculations. Regardless of the mechanism, further studies are needed to ascertain the generalizability of these effects beyond acenes; it should be possible to design molecules with deliberate strong, intermolecular $\pi-\pi$ interactions optimized for differences in packing across various substrates. Moreover, the static nature of SAM-based junctions means that such effects could be exploited in devices, for example, by designing molecular switches capable of forming and breaking strong intermolecular contacts reversibly.

■ ASSOCIATED CONTENT

Supporting Information

The Supporting Information is available free of charge at https://pubs.acs.org/doi/10.1021/acs.jpcc.0c05781.

Experimental details, electrical characterization, surface characterization, and computational details, and coordinates (PDF)

■ AUTHOR INFORMATION

Corresponding Authors

Herre S. J. van der Zant − *Kavli Institute of Nanoscience, Delft University of Technology, Delft 2628, CJ, The Netherlands;* orcid.org/0000-0002-5385-0282; Email: h.s.j.vanderzant@tudelft.nl

Ryan C. Chiechi − *Stratingh Institute for Chemistry and Zernike Institute for Advanced Materials, University of Groningen, 9747, AG, Groningen, The Netherlands;* orcid.org/0000-0002-0895-2095; Email: r.c.chiechi@rug.nl

Authors

Yuru Liu − *Stratingh Institute for Chemistry and Zernike Institute for Advanced Materials, University of Groningen, 9747, AG, Groningen, The Netherlands*

Luca Ornago − *Kavli Institute of Nanoscience, Delft University of Technology, Delft 2628, CJ, The Netherlands*

Marco Carlotti − *Stratingh Institute for Chemistry and Zernike Institute for Advanced Materials, University of Groningen, 9747, AG, Groningen, The Netherlands*

Yong Ai − *Stratingh Institute for Chemistry and Zernike Institute for Advanced Materials, University of Groningen, 9747, AG, Groningen, The Netherlands*

Maria El Abbassi − *Kavli Institute of Nanoscience, Delft University of Technology, Delft 2628, CJ, The Netherlands;* orcid.org/0000-0001-5177-6528

Saurabh Soni − *Stratingh Institute for Chemistry and Zernike Institute for Advanced Materials, University of Groningen, 9747, AG, Groningen, The Netherlands;* orcid.org/0000-0002-8159-9128

Andika Asyuda − *Angewandte Physikalische Chemie, Universität Heidelberg, D-69120 Heidelberg, Germany*

Michael Zharnikov − *Angewandte Physikalische Chemie, Universität Heidelberg, D-69120 Heidelberg, Germany;* orcid.org/0000-0002-3708-7571

Complete contact information is available at: https://pubs.acs.org/10.1021/acs.jpcc.0c05781

Notes

The authors declare no competing financial interest.

■ ACKNOWLEDGMENTS

R.C.C., M.C., and Y.A. acknowledge the European Research Council for the ERC Starting Grant 335473 (MOLECSYNCON). Y.L. acknowledges financial support from the China

Scholarship Council (CSC): NO.201707040075. S.S. acknowledges the Zernike Institute for Advanced Materials. The work at Delft was in part supported by the EC H2020 FET Open project 767187 (QuIET). We thank Dr. Harry. T. Jonkman for his help with angle-resolved XPS experiments. We acknowledge Dr. Remco W. A. Havenith for help with the ADF calculations and NWO for access to the Dutch national e-infrastructure. Part of this work was carried out on the Dutch national e-infrastructure (Cartesius) with the support of SURF Cooperative. We thank the Center for Information Technology of the University of Groningen for their support and for providing access to the Peregrine high performance computing cluster. A.A. and M.Z thank the Helmholtz Zentrum Berlin for the allocation of synchrotron radiation beamtime at BESSY II and financial support as well as A. Nefedov and Ch. Wöll for the technical cooperation during the experiments at BESSY II. We thank E. Sauter for participation in some of the experiments in context of this project. A.A. acknowledges the financial support by the DAAD-ACEH Scholarship of Excellence. L.O. acknowledges A. Rates for the support on data analysis scripts.

REFERENCES

(1) Vilan, A.; Aswal, D.; Cahen, D. Large-Area, Ensemble Molecular Electronics: Motivation and Challenges. *Chem. Rev.* **2017**, *117*, 4248−4286.

(2) Xiang, L.; Hines, T.; Palma, J. L.; Lu, X.; Mujica, V.; Ratner, M. A.; Zhou, G.; Tao, N. Non-Exponential Length Dependence of Conductance in Iodide-Terminated Oligothiophene Single-Molecule Tunneling Junctions. *J. Am. Chem. Soc.* **2016**, *138*, 679−687.

(3) Xin, N.; Guo, X. Catalyst: The Renaissance of Molecular Electronics. *Chem.* **2017**, *3*, 373−376.

(4) Lörtscher, E. Reaction: Technological Aspects of Molecular Electronics. *Chem.* **2017**, *3*, 376−377.

(5) Aviram, A.; Ratner, M. A. Molecular Rectifiers. *Chem. Phys. Lett.* **1974**, *29*, 277−283.

(6) Solomon, G. C.; Herrmann, C.; Vura-Weis, J.; Wasielewski, M. R.; Ratner, M. A. The Chameleonic Nature of Electron Transport Through Π-Stacked Systems. *J. Am. Chem. Soc.* **2010**, *132*, 7887−7889.

(7) Markussen, T.; Stadler, R.; Thygesen, K. S. The Relation Between Structure and Quantum Interference in Single Molecule Junctions. *Nano Lett.* **2010**, *10*, 4260−4265.

(8) Tsuji, Y.; Hoffmann, R.; Movassagh, R.; Datta, S. Quantum Interference in Polyenes. *J. Chem. Phys.* **2014**, *141*, 224311.

(9) Fracasso, D.; Valkenier, H.; Hummelen, J. C.; Solomon, G. C.; Chiechi, R. C. Evidence for Quantum Interference in SAMs of Arylethynylene Thiolates in Tunneling Junctions With Eutectic Ga−In (EGaIn) Top-Contacts. *J. Am. Chem. Soc.* **2011**, *133*, 9556−9563.

(10) Pedersen, K. G. L.; Borges, A.; Hedegård, P.; Solomon, G. C.; Strange, M. Illusory Connection Between Cross-Conjugation and Quantum Interference. *J. Phys. Chem. C* **2015**, *119*, 26919−26924.

(11) Zhang, Y.; Ye, G.; Soni, S.; Qiu, X.; Krijger, T. L.; Jonkman, H. T.; Carlotti, M.; Sauter, E.; Zharnikov, M.; Chiechi, R. C. Controlling Destructive Quantum Interference in Tunneling Junctions Comprising Self-Assembled Monolayers via Bond Topology and Functional Groups. *Chem. Sci.* **2018**, *9*, 4414−4423.

(12) Carlotti, M.; Soni, S.; Qiu, X.; Sauter, E.; Zharnikov, M.; Chiechi, R. C. Systematic Experimental Study of Quantum Interference Effects in Anthraquinoid Molecular Wires. *Nanoscale Advances* **2019**, *1*, 2018−2028.

(13) Manrique, D. Z.; Huang, C.; Baghernejad, M.; Zhao, X.; Al-Owaedi, O. A.; Sadeghi, H.; Kaliginedi, V.; Hong, W.; Gulcur, M.; Wandlowski, T.; et al. A Quantum Circuit Rule for Interference Effects in Single-Molecule Electrical Junctions. *Nat. Commun.* **2015**, *6*, 6389.

(14) Gantenbein, M.; Wang, L.; Al-jobory, A. A.; Ismael, A. K.; Lambert, C. J.; Hong, W.; Bryce, M. R. Quantum Interference and Heteroaromaticity of Para-And Meta-Linked Bridged Biphenyl Units in Single Molecular Conductance Measurements. *Sci. Rep.* **2017**, *7*, 1794.

(15) Stefani, D.; Weiland, K. J.; Skripnik, M.; Hsu, C.; Perrin, M. L.; Mayor, M.; Pauly, F.; van der Zant, H. S. Large Conductance Variations in a Mechanosensitive Single-Molecule Junction. *Nano Lett.* **2018**, *18*, 5981−5988.

(16) Carlotti, M.; Kovalchuk, A.; Wächter, T.; Qiu, X.; Zharnikov, M.; Chiechi, R. C. Conformation-Driven Quantum Interference Effects Mediated by Through-Space Conjugation in Self-Assembled Monolayers. *Nat. Commun.* **2016**, *7*, 13904.

(17) Valkenier, H.; Huisman, E. H.; van Hal, P. A.; de Leeuw, D. M.; Chiechi, R. C.; Hummelen, J. C. Formation of High-Quality Self-Assembled Monolayers of Conjugated Dithiols on Gold: Base Matters. *J. Am. Chem. Soc.* **2011**, *133*, 4930−4939.

(18) Kaliginedi, V.; Moreno-García, P.; Valkenier, H.; Hong, W.; García-Suárez, V. M.; Buiter, P.; Otten, J. L. H.; Hummelen, J. C.; Lambert, C. J.; Wandlowski, T. Correlations Between Molecular Structure and Single-Junction Conductance: A Case Study With Oligo(phenylene-Ethynylene)-Type Wires. *J. Am. Chem. Soc.* **2012**, *134*, 5262−5275.

(19) Frisenda, R.; Stefani, D.; van der Zant, H. S. J. Quantum Transport Through a Single Conjugated Rigid Molecule, a Mechanical Break Junction Study. *Acc. Chem. Res.* **2018**, *51*, 1359−1367.

(20) Bendikov, M.; Duong, H. M.; Starkey, K.; Houk, K. N.; Carter, E. A.; Wudl, F. Oligoacenes Theoretical Prediction of Open-Shell Singlet Diradical Ground States. *J. Am. Chem. Soc.* **2004**, *126*, 7416−7417.

(21) Kim; Beebe, J. M.; Jun, Y.; Zhu, X.-Y.; Frisbie, C. D. Correlation Between HOMO Alignment and Contact Resistance in Molecular Junctions: Aromatic Thiols Versus Aromatic Isocyanides. *J. Am. Chem. Soc.* **2006**, *128*, 4970−4971.

(22) Yelin, T.; Korytár, R.; Sukenik, N.; Vardimon, R.; Kumar, B.; Nuckolls, C.; Evers, F.; Tal, O. Conductance Saturation in a Series of Highly Transmitting Molecular Junctions. *Nat. Mater.* **2016**, *15*, 444−449.

(23) Cirera, B.; Sánchez-Grande, A.; de la Torre, B.; Santos, J.; Edalatmanesh, S.; Rodríguez-Sánchez, E.; Lauwaet, K.; Mallada, B.; Zbořil, R.; Miranda, R.; et al. Tailoring topological order and π-conjugation to engineer quasi-metallic polymers. *Nat. Nanotechnol.* **2020**, *15*, 437−443.

(24) Klare, J. E.; Tulevski, G. S.; Sugo, K.; de Picciotto, A.; White, K. A.; Nuckolls, C. Cruciform π-Systems for Molecular Electronics Applications. *J. Am. Chem. Soc.* **2003**, *125*, 6030−6031.

(25) Miao, Q.; Chi, X.; Xiao, S.; Zeis, R.; Lefenfeld, M.; Siegrist, T.; Steigerwald, M. L.; Nuckolls, C. Organization of Acenes With a Cruciform Assembly Motif. *J. Am. Chem. Soc.* **2006**, *128*, 1340−1345.

(26) Valkenier, H.; Guédon, C. M.; Markussen, T.; Thygesen, K. S.; van der Molen, S. J.; Hummelen, J. C. Cross-Conjugation and Quantum Interference: A General Correlation? *Phys. Chem. Chem. Phys.* **2014**, *16*, 653−662.

(27) Weiss, E. A.; Kaufman, G. K.; Kriebel, J. K.; Li, Z.; Schalek, R.; Whitesides, G. M. Si/SiO2-Templated Formation of Ultraflat Metal Surfaces on Glass, Polymer, and Solder Supports: Their Use as Substrates for Self-Assembled Monolayers. *Langmuir* **2007**, *23*, 9686−9694.

(28) Qiu, L.; Zhang, Y.; Krijger, T. L.; Qiu, X.; van't Hof, P.; Hummelen, J. C.; Chiechi, R. C. Rectification of Current Responds to Incorporation of Fullerenes Into Mixed-Monolayers of Alkanethiolates in Tunneling Junctions. *Chem. Sci.* **2017**, *8*, 2365−2372.

(29) Nefedov, A.; Wöll, C. *Surface Science Techniques*; Springer: Berlin, Heidelberg, 2013; pp 277−303.

(30) Moulder, J.; Stickle, W.; Sobol, P.; Bomben, K. In *Handbook of X-Ray Photoelectron Spectroscopy*; Chastain, J., Ed.; Perkin-Elmer Corporation: Eden Prairie, MN, 1992.

https://dx.doi.org/10.1021/acs.jpcc.0c05781
J. Phys. Chem. C 2020, 124, 22776−22783

(31) Simeone, F. C.; Yoon, H. J.; Thuo, M. M.; Barber, J. R.; Smith, B.; Whitesides, G. M. Defining the Value of Injection Current and Effective Electrical Contact Area for EGaIn-Based Molecular Tunneling Junctions. *J. Am. Chem. Soc.* **2013**, *135*, 18131−18144.
(32) Martin, C. A.; Smit, R. H. M.; van Egmond, R.; van der Zant, H. S. J.; van Ruitenbeek, J. M. A Versatile Low-Temperature Setup for the Electrical Characterization of Single-Molecule Junctions. *Rev. Sci. Instrum.* **2011**, *82*, 053907.
(33) Neese, F. The ORCA Program System. *Wiley Interdiscip. Rev.: Comput. Mol. Sci.* **2012**, *2*, 73−78.
(34) Neese, F. Software Update: The ORCA Program System, Version 4.0. *Sci. China, Ser. F: Info. Sci.* **2017**, *8*, No. e1327.
(35) Herrmann, C.; Solomon, G. C.; Subotnik, J. E.; Mujica, V.; Ratner, M. A. Ghost Transmission: How Large Basis Sets Can Make Electron Transport Calculations Worse. *J. Chem. Phys.* **2010**, *132*, 024103.
(36) Deffner, M.; Gross, L.; Steenbock, T.; Voigt, B. A.; Solomon, G. C.; Herrmann, C. ARTAIOS - a transport code for postprocessing quantum chemical electronic structure calculations, available from https://www.chemie.uni-hamburg.de/institute/ac/arbeitsgruppen/herrmann/software/artaios.html; Aug 30, 2018.
(37) Philipsen, P.; te Velde, G.; Baerends, E.; Berger, J.; de Boeij, P.; Franchini, M.; Groeneveld, J.; Kadantsev, E.; Klooster, R.; Kootstra, F.; et al. *P. R. BAND 2019.3, SCM, Theoretical Chemistry*; Vrije Universiteit: Amsterdam, The Netherlands, http://www.scm.com, Sep 11, 2019.
(38) Nerngchamnong, N.; Yuan, L.; Qi, D.-C.; Li, J.; Thompson, D.; Nijhuis, C. A. The Role of Van Der Waals Forces in the Performance of Molecular Diodes. *Nat. Nanotechnol.* **2013**, *8*, 113−118.
(39) Chiechi, R.; Weiss, E.; Dickey, M.; Whitesides, G. Eutectic Gallium−Indium (EGaIn): A Moldable Liquid Metal for Electrical Characterization of Self-Assembled Monolayers. *Angew. Chem., Int. Ed.* **2008**, *47*, 142−144.
(40) Krijger, T. L. The Soft Molecular Landing Machine Ultra-High Vacuum Deposition of Non-Volatile Solution Processable Organic Materials and Polymers. *Ph.D. dissertation*, University of Groningen, 2018.
(41) Schreiber, F. Structure and Growth of Self-Assembling Monolayers. *Prog. Surf. Sci.* **2000**, *65*, 151−257.
(42) Hutt, D. A.; Leggett, G. J. Influence of Adsorbate Ordering on Rates of UV Photooxidation of Self-Assembled Monolayers. *J. Phys. Chem.* **1996**, *100*, 6657−6662.
(43) Schoenfisch, M. H.; Pemberton, J. E. Air Stability of Alkanethiol Self-Assembled Monolayers on Silver and Gold Surfaces. *J. Am. Chem. Soc.* **1998**, *120*, 4502−4513.
(44) Nilsson, D.; Watcharinyanon, S.; Eng, M.; Li, L.; Moons, E.; Johansson, L. S. O.; Zharnikov, M.; Shaporenko, A.; Albinsson, B.; Mårtensson, J. Characterization of Self-Assembled Monolayers of Oligo(phenyleneethynylene) Derivatives of Varying Shapes on Gold: Effect of Laterally Extended π-Systems. *Langmuir* **2007**, *23*, 6170−6181.
(45) He, J.; Sankey, O.; Lee, M.; Tao, N.; Li, X.; Lindsay, S. Measuring Single Molecule Conductance With Break Junctions. *Faraday Discuss.* **2006**, *131*, 145−154.
(46) Frisenda, R.; Perrin, M. L.; Valkenier, H.; Hummelen, J. C.; van der Zant, H. S. Statistical Analysis of Single-Molecule Breaking Traces. *Phys. Status Solidi B* **2013**, *250*, 2431−2436.
(47) Wu, S.; González, M. T.; Huber, R.; Grunder, S.; Mayor, M.; Schönenberger, C.; Calame, M. Molecular Junctions Based on Aromatic Coupling. *Nat. Nanotechnol.* **2008**, *3*, 569.
(48) Cabosart, D.; El Abbassi, M.; Stefani, D.; Frisenda, R.; Calame, M.; Van der Zant, H. S.; Perrin, M. L. A Reference-Free Clustering Method for the Analysis of Molecular Break-Junction Measurements. *Appl. Phys. Lett.* **2019**, *114*, 143102.
(49) Abbassi, M. E.; Zwick, P.; Rates, A.; Stefani, D.; Prescimone, A.; Mayor, M.; van der Zant, H. S. J.; Dulić, D. Unravelling the Conductance Path Through Single-Porphyrin Junctions. *Chem. Sci.* **2019**, *10*, 8299−8305.
(50) Frisenda, R.; Janssen, V. A. E. C.; Grozema, F. C.; van der Zant, H. S. J.; Renaud, N. Mechanically Controlled Quantum Interference in Individual Π-Stacked Dimers. *Nat. Chem.* **2016**, *8*, 1099−1104.
(51) Carlotti, M.; Soni, S.; Kumar, S.; Ai, Y.; Sauter, E.; Zharnikov, M.; Chiechi, R. C. Two-Terminal Molecular Memory Through Reversible Switching of Quantum Interference Features in Tunneling Junctions. *Angew. Chem., Int. Ed.* **2018**, *57*, 15681−15685.
(52) Pourhossein, P.; Vijayaraghavan, R. K.; Meskers, S. C.; Chiechi, R. C. Optical Modulation of Nano-Gap Tunnelling Junctions Comprising Self-Assembled Monolayers of Hemicyanine Dyes. *Nat. Commun.* **2016**, *7*, 11749.
(53) Weiss, E. A.; Chiechi, R. C.; Kaufman, G. K.; Kriebel, J. K.; Li, Z.; Duati, M.; Rampi, M. A.; Whitesides, G. M. Influence of Defects on the Electrical Characteristics of Mercury-Drop Junctions: Self-Assembled Monolayers Ofn-Alkanethiolates on Rough and Smooth Silver. *J. Am. Chem. Soc.* **2007**, *129*, 4336−4349.
(54) Guédon, C. M.; Valkenier, H.; Markussen, T.; Thygesen, K. S.; Hummelen, J. C.; van der Molen, S. J. Observation of Quantum Interference in Molecular Charge Transport. *Nat. Nanotechnol.* **2012**, *7*, 305−309.
(55) Dubi, Y. Transport Through Self-Assembled Monolayer Molecular Junctions: Role of In-Plane Dephasing. *J. Phys. Chem. C* **2014**, *118*, 21119−21127.
(56) Obersteiner, V.; Egger, D. A.; Heimel, G.; Zojer, E. Impact of Collective Electrostatic Effects on Charge Transport through Molecular Monolayers. *J. Phys. Chem. C* **2014**, *118*, 22395−22401.
(57) Yoshizawa, K.; Tada, T.; Staykov, A. Orbital Views of the Electron Transport in Molecular Devices. *J. Am. Chem. Soc.* **2008**, *130*, 9406−9413.
(58) Solomon, G. In *Handbook of single-molecule electronics*; Moth-Poulsen, K., Ed.; CRC Press, 2015; pp 341−369.

https://dx.doi.org/10.1021/acs.jpcc.0c05781
J. Phys. Chem. C 2020, 124, 22776−22783